analytical chemistry

pubs.acs.org/ac

Article

Ultrastable Silver Nanoparticles for Rapid Serology Detection of Anti-SARS-CoV-2 Immunoglobulins G

Bryan Gosselin,[#] Maurice Retout,[#] Raphaël Dutour, Ludovic Troian-Gautier, Robin Bevernaegie, Sophie Herens, Philippe Lefèvre, Olivier Denis, Gilles Bruylants,* and Ivan Jabin*

Cite This: *Anal. Chem.* 2022, 94, 7383−7390

Read Online

ACCESS | Metrics & More | Article Recommendations | Supporting Information

ABSTRACT: Dipstick assays using silver nanoparticles (AgNPs) stabilized by a thin calix[4]arene-based coating were developed and used for the detection of Anti-SARS-CoV-2 IgG in clinical samples. The calixarene-based coating enabled the covalent bioconjugation of the SARS-CoV-2 Spike Protein via the classical EDC/sulfo-NHS procedure. It further conferred remarkable stability to the resulting bioconjugated AgNPs, as no degradation was observed over several months. In comparison with lateral-flow immunoassays (LFIAs) based on classical gold nanoparticles, our AgNP-based system constitutes a clear step forward, as the limit of detection for Anti-SARS-CoV-2 IgG was reduced by 1 order of magnitude and similar signals were observed with 10 times fewer particles. In real clinical samples, the AgNP-based dipstick assays showed impressive results: 100% specificity was observed for negative samples, while a sensitivity of 73% was determined for positive samples. These values match the typical sensitivities obtained for reported LFIAs based on gold nanoparticles. These results (i) represent one of the first examples of the use of AgNP-based dipstick assays in the case of real clinical samples, (ii) demonstrate that ultrastable calixarene-coated AgNPs could advantageously replace AuNPs in LFIAs, and thus (iii) open new perspectives in the field of rapid diagnostic tests.

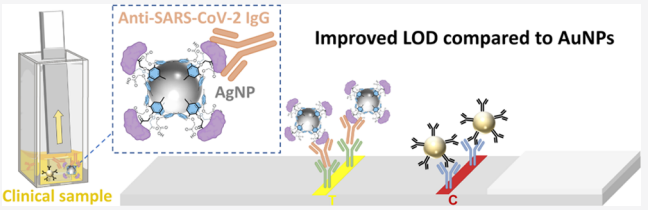

1. INTRODUCTION

The enzyme-linked immunosorbent assay (ELISA) is commonly used as a serological test for detecting proteins (e.g., biomarkers, antibodies). If ELISAs enable an accurate and sensitive detection, they however suffer from severe drawbacks including high production cost, long experiment time, and the need for trained operators.[1] The COVID-19 crisis has shown that the development of alternative point-of-care (POC) methods allowing a convenient and rapid screening is urgently required.[2] Among all of the rapid diagnostic tests (RDTs) developed over the past years, lateral-flow immunoassays (LFIAs) are probably the most widely used.[3−6] Indeed, LFIAs combine all of the POC features such as simple read-out signal (naked eye observation), low cost, and ease of use.[7]

Gold nanoparticles (AuNPs) are classically used as the colorimetric reporter in LFIAs because they exhibit a localized surface plasmon resonance (LSPR) band in the visible region and absorb light with an extinction coefficient higher by at least 3 orders of magnitude than any organic molecule.[8,9] In addition, their synthesis[10] as well as their surface modification with biomolecules[11−13] are well established. Nevertheless, if compared to ELISAs that often exhibit a limit of detection (LOD) in the nanomolar to picomolar range,[14] current AuNP-based LFIAs suffer from a poor sensitivity (LOD in the micromolar range). Recent efforts to improve the sensitivity of LFIAs have focused on signal amplification or on the use of a secondary signal obtained through fluorescence, surface-enhanced Raman spectroscopy, or electrochemistry.[15−17] Unfortunately, most of these approaches require additional steps or supplementary equipment, which is not compatible with point-of-care testing.

To address this, we envisioned the use of a colorimetric reporter that would exhibit better optical properties than AuNPs, as it would not increase the assay time or its complexity. In this regard, silver nanoparticles (AgNPs) are plasmonic nanoparticles that also display an LSPR band in the visible region but with an extinction coefficient 1 order of magnitude higher than the one of AuNPs of similar size. AgNPs could therefore lead to more sensitive LFIAs than AuNPs.[18] Their use has however been scarcely reported for the detection of proteins.[19,20] It is in part due to the weak chemical and colloidal stabilities of AgNPs in complex media or over time.[21] In contrast to AuNPs, AgNPs are indeed very sensitive to oxidation and their conjugation with biomolecules is thus difficult to achieve without important particles loss or

Received: February 22, 2022
Accepted: May 2, 2022
Published: May 13, 2022

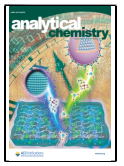

degradation.[20−22] Moreover, their dispersion in biological fluids remains highly challenging.

Calix[4]arene-based coatings have recently been shown to drastically improve the colloidal stability of AgNPs compared to commercially available ones.[23] These coatings are easily obtained via the irreversible reduction of calix[4]arene-tetradiazonium salts, leading to robust and thin organic monolayers (with a typical thickness of ca. 2 nm).[24−26] In addition, we have shown that these ultrastable AgNPs can be easily manipulated and conjugated to biomolecules such as proteins.[27] In this global pandemic context, we envisioned that calixarene-coated AgNPs could be advantageously used as a colorimetric reporter in LFIA for the detection of anti-SARS-CoV-2 immunoglobulins G (Anti-SARS-CoV-2 IgG). To date, more than 400 million people have been infected by SARS-CoV-2, causing more than 5.79 million reported deaths and making COVID-19 one of the worst plagues of the 21st century (based on Johns Hopkins University data). Serological LFIAs using gold nanoparticles were rapidly and widely commercialized, as they enable the detection of IgM and IgG that are produced 3−6 days and 8 days after coronavirus infection, respectively.[28] Our hope was that AgNP-based LFIAs would lead to a more reliable and efficient serological test with lower detection limits than AuNP-based LFIAs.[1]

Herein, we show with a dipstick design that calixarene-coated silver nanoparticles are valuable candidates for the development of LFIAs able to detect Anti-SARS-CoV-2 IgG in buffer, human plasma, and real clinical samples.

2. MATERIALS AND METHODS

2.1. Chemical and Biomolecules. All chemicals were at least of reagent grade. Recombinant SARS-CoV-2 RBD Spike Protein was obtained from RayBiotech (230-30162), and Goat Anti-human IgG was obtained from Sigma-Aldrich (I2136). Fully human SARS-CoV-2 IgG was purchased from GeneTech. Blocker casein buffer (PBS) was obtained from Thermo Fisher, and bovine serum albumin (BSA) >98% was from Sigma-Aldrich. Rabbit IgG (PP64) and Goat Anti-Rabbit IgG (SAB3700848) were obtained from Sigma-Aldrich. Commercial Prot A/G dipsticks were obtained from Abcam as part of "Check and go" conjugation kit. NC membranes were obtained from Cytiva for HP170 and Sartorius for CN140. Absorbent Pads SureWick (1.7 × 30 cm^2) were purchased from Sigma-Aldrich. The synthesis of the calix[4]arene-tetraacid tetradiazonium salt X_4 was achieved according to the literature[29] from commercially available *p*-*t*Bu-calix[4]arene (note however that the reduction of the nitro groups of the intermediate tetra-nitro derivative was achieved through hydrogenation (H_2, Pd/C) and not by using $SnCl_2$, as it was previously described). AuNPs-citrate with a mean core diameter between 15 and 20 nm was synthesized following a previously reported procedure.[30]

2.2. Characterizations and Measurements. UV−vis absorption spectra were recorded with a UV−vis spectrophotometer in disposable semi-micro cuvettes (PMMA). As-synthesized NPs were diluted by a factor of 10 in 1 mL of aqueous solution, unless otherwise noted. Attenuated total reflection Fourier-transform infrared (ATR-FTIR) spectra were recorded at 20 °C on an FTIR spectrophotometer equipped with a liquid-nitrogen-cooled mercury−cadmium−telluride (MCT) detector. The silver nanoparticles were centrifugated, and 2 μL of the pellet was deposited on a germanium internal reflection element (triangular prism of 6.8 × 45 mm^2 with an internal angle of incidence of 45°). Water was removed with a flow of nitrogen gas. Opus software (4.2.37) was used to record 128 scans with a resolution of 2 cm^{-1} under a continuous flow of nitrogen gas over the sample. Data were processed and analyzed using the Kinetics software in MatLab 7.1 (Mathworks, Inc., Natick, MA) by the subtraction of water vapor, baseline correction, apodization at 4 cm^{-1}, and flattening of the CO_2 signal. Finally, the spectra were normalized at 1459 cm^{-1} (aromatic ring stretching band from the calixarenes) to compensate for variations in the number of AgNPs present on the spot of the Ge crystal where the measurement was performed. Images of the AgNPs/AuNPs were obtained with a transmission electron microscope (TEM) equipped with a lanthanum hexaboride (LaB6) crystal at a 200 kV accelerating voltage. The average size and standard deviation were determined by measuring the size of more than 150 NPs for each sample. Samples were characterized by dynamic light scattering (DLS) with back scattering (NIBS 173°). Measurements were performed at 25 °C using a refractive index of 1.34 for the silver nanoparticles. AgNPs (5 μL ∼ 1 nM) were dispersed in LiChrosolv water to obtain 1 mL of AgNPs (∼0.05 nM) in disposable semi-micro cuvettes (PMMA), and multiple DLS measurements were performed. The reported values are the average hydrodynamic diameter obtained from three independent measurements using the Z average as calculated by the Zetasizer software.

2.3. Synthesis of AgNPs-X_4. AgNPs-X_4 were synthesized following a previously reported procedure.[23] In a Protein LoBind 50 mL Falcon, 3 mL of $AgNO_3$ (10 mM) was mixed with 7.2 mL of an aqueous solution of calixarene X_4 (5 mM). LiChrosolv water (11.5 mL) was then added. Finally, the pH was adjusted to 6.5 through the addition of the appropriate volume of 1 M NaOH and, rapidly after this, 8.2 mL of sodium ascorbate was added. The resulting mixture was then heated at 60 °C and stirred at 1000 rpm using a thermomixer. After 16 h of reaction, 60 μL of 1 M NaOH was added into the tube. The Falcon was then centrifugated at 18 000*g* for 20 min. The supernatant was discarded, and the particles were resuspended in a 5 mM NaOH solution. This washing cycle was repeated three times except that after the last centrifugation, the NPs were resuspended in Milli-Q H_2O rather than in a 5 mM NaOH solution. The resulting AgNPs-X_4 were stored at room temperature.

2.4. Preparation of AgNPs-X_4-Prot-S or AgNPs-X_4-Goat IgG. In a 1.5 mL Protein LoBind Eppendorf, 500 μL of AgNP-X_4 (OD = 6.2), 50 μL of MES buffer (100 mM, pH 5.8), 10 μL of 1-ethyl-3-(3-dimethylaminopropyl)carbodiimide chlorohydrate (EDC·HCl) (6 mM), and 10 μL of *N*-hydroxysulfosuccinimide (sulfo-NHS) (10 mM) were added successively. The activation step was carried out for 1 h, and the activated nanoparticles were centrifugated once (15 min, 15 000*g*). The supernatant was discarded. The pellets were resuspended in Milli-Q H_2O (500 μL) and then transferred into a 1.5 mL glass vial. Then, 50 μL of goat IgG (0.2 mg/mL) or 3 μL of SARS-CoV-2 recombinant protein (30 μM) were added, and the reaction mixture was stirred for 4 h at 1000 rpm at room temperature. 1% Casein (0.1 mL) in 100 mM phosphate buffer (PB) pH 7.4 (with 150 mM NaCl) was added to the solution to block the AgNP surface. After incubation for 5 min at room temperature, the mixture was centrifuged at 15 000*g* for 20 min. The supernatant was discarded, and the AgNP conjugate was resuspended in 1.5 mL of 0.1% casein in 10 mM PB (with 15 mM NaCl). The

https://doi.org/10.1021/acs.analchem.2c00870
Anal. Chem. 2022, 94, 7383−7390

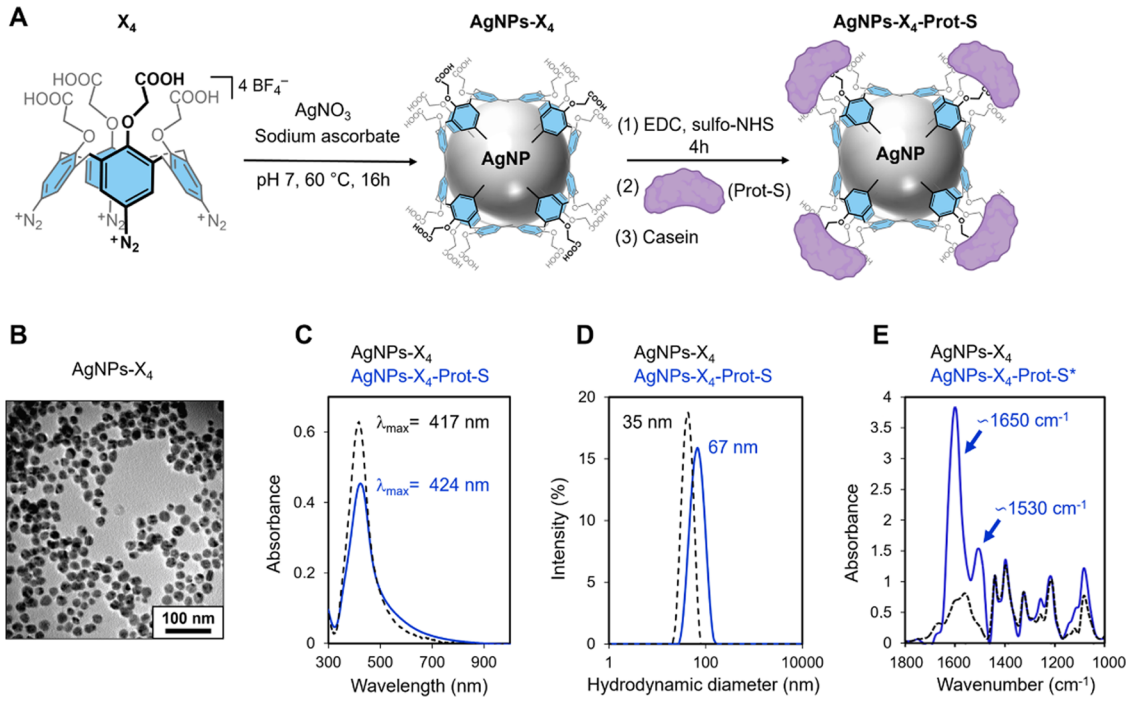

Figure 1. (A) Illustration of the synthesis of AgNPs-X_4-Prot-S. Note that the representation of the NP is schematic, as all calixarenes are not necessarily attached with four bonds to the surface and each Prot-S could be linked to multiple calixarenes. (B) TEM image of AgNPs-X_4. (C) UV−vis spectra recorded in water at pH 7 for AgNPs-X4, before and after the coupling of Prot-S (AgNPs-X4-ProtS). (D) Average hydrodynamic diameter obtained by DLS in water at pH 7. (E) IR spectra of AgNPs-X_4 (black dashed line) and AgNPs-X_4-Prot-S (blue plain line); *: before the addition of casein.

centrifugation and resuspension cycle was repeated twice, and the final suspension solution was resuspended in 1× PBS. The resulting AgNPs-X_4-Prot-S or AgNPs-X_4-Goat IgG was stored at 4 °C.

2.5. Preparation of AuNPs-Citrate-Prot-S, AuNPs-Citrate-Goat IgG, or AuNPs-Citrate-Rabbit IgG. SARS-CoV-2 recombinant protein (10 μL, 30 μM), goat IgG (20 μL, 2 mg/mL), or rabbit IgG (20 μL, 2 mg/mL in 1× PBS) were added to a mixture of 1 mL of AuNPs-citrate (OD = 2) and 0.1 mL of borate buffer (0.1 M, pH 8.5). After incubation for 2 h at room temperature, 0.1 mL of 1% casein in 100 mM phosphate buffer pH 7.4 (with 150 mM NaCl) was added to the solution to block the AuNP surface. After incubation for 15 min at room temperature, the mixture was centrifuged at 15 000*g* for 20 min. The supernatant was discarded and the AuNP conjugate was resuspended in 1.5 mL of 0.1% casein in 10 mM phosphate buffer pH 7.4 (with 15 mM NaCl). The centrifugation and resuspension cycle was repeated twice, and the final suspension solution was resuspended in 400 μL of 1× PBS. The resulting AuNPs-citrate-Prot-S, AuNPs-citrate-Goat IgG, or AuNPs-citrate-Rabbit IgG was stored at 4 °C.

2.6. Dipstick Assembly. Anti-Rabbit IgG (2 mg/mL) was immobilized on the nitrocellulose membrane as the control line (C), and Goat Anti-Human IgG (2 mg/mL) was immobilized as the test line (T). The NC membrane was dried for 2 h at 37 °C and was then incubated for 10 min in the appropriate blocking buffer: 0.5% Casein or 1% BSA in water. After incubation, NC membranes were washed five times with Milli-Q H_2O and dried at 37 °C for 2 h. Then, the absorbent pad was added on the NC membrane (with an overlap of 3 mm). The dipstick was cut into 5 mm strips and stored in a desiccator.

2.7. Dipstick Assay Procedure. In a disposable cuvette, 40 μL of running buffer (5% BSA, 0.2% Tween 20, 1% PEG-6000 in 0.5× PBS) and 10 μL of AgNP-X_4-Prot-S (OD = 5) were mixed with 10 μL of plasma. After 15 min, the dipstick was partially immersed in the solution and readout was performed after 15 min.

2.8. Sample Collection. Serum samples were collected in the "Princesse Paola Hospital" of Marche-en-Famenne and in the "Sainte-Thérèse Hospital" of Bastogne from March 27 to May 4, 2020. Permission to conduct this study was obtained from the Ethics Committee of the VIVALIA Hospital group (study OM 152). Positive samples were obtained from adult patients who tested positive for SARS-CoV-2 by PCR. Written informed consent was signed for all patients by patients themselves or by their legal representative if they were unable to give it. Control serums were collected at the beginning of January 2020 before the emergence of the SARS-CoV-2 in Belgium from a group of patients without any respiratory/infectious diseases.

2.9. ELISA Procedure. Total and IgM antibodies specific for the receptor-binding domain of SARS-CoV-2 spike protein were analyzed using the Wantai SARS-CoV-2 Ab ELISA (Wantai Biological Pharmacy, Beijing, China) (Wantai ELISA) following the manufacturer's recommendations. Results were calculated by relating each specimen absorbance value to the cutoff value obtained from the absorbance of three negative calibrators. Results with a ratio greater than 1 are considered positive. Spike (S1/S2) specific IgG antibodies were analyzed using the LIAISON SARS-CoV-2 IgG kit (DiaSorin S.p.A., Saluggia, Italy). This assay was performed on a LIAISON XL Analyzer according to the manufacturer's instructions. The obtained results are quantitative and given as arbitrary units

https://doi.org/10.1021/acs.analchem.2c00870
Anal. Chem. 2022, 94, 7383−7390

Scheme 1. Dipstick Assay Principle for the Detection of Anti-SARS-CoV-2 IgG with Calixarene-Coated AgNPs[a]

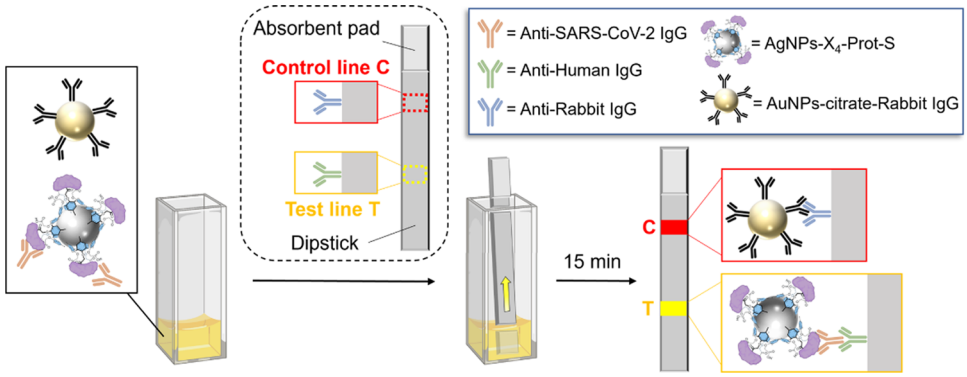

[a]A mixture containing AgNPs-X_4-Prot-S and AuNPs-citrate-Rabbit IgG is first incubated with a plasma sample containing Anti-SARS-CoV-2 IgG. After immersion of the dipstick and migration of the solution, the test line (T) and control line (C) are easily observed with the unaided eye as a yellow-colored line and a red-colored line, respectively.

per milliliter (AU/mL). Values <12 AU/mL are considered negative.

3. RESULTS AND DISCUSSION

3.1. Preparation and Characterization of Calix[4]-arene-Coated Silver Nanoparticles. Readily available calix[4]arene-tetraacid tetradiazonium salt (X_4)[29] was deemed the ideal candidate for the development of dipstick devices as its four carboxyl groups can be covalently conjugated to proteins (Figure 1A). First, the corresponding calix[4]arene-coated silver nanoparticles (AgNPs-X_4) were obtained via the reduction of silver nitrate in the presence of calixarene X_4.[23] AgNPs-X_4 were then conjugated to the receptor-binding domain (RBD) of the SARS-CoV-2 Spike Protein (Prot-S) via the classical EDC/sulfo-NHS procedure. After conjugation, the surface of the nanoparticles was blocked with casein to avoid further nonspecific binding of endogenous proteins. The resulting nanoparticles AgNPs-X_4-Prot-S were thoroughly washed through several centrifugation/resuspension cycles and finally suspended in phosphate-buffered saline (1× PBS) solution.

The nanoparticles AgNPs-X_4 and AgNPs-X_4-Prot-S were characterized by UV−vis and IR spectroscopies as well as by dynamic light scattering (DLS) and transmission electron microscopy (TEM). TEM analysis of AgNPs-X_4 revealed spherical monodisperse particles with a core size of 22 ± 3 nm (Figure 1B). AgNPs-X_4 exhibited a sharp and intense LSPR band with a maximum (λ_{max}) centered at 417 nm, conferring to the suspension a bright yellow color (Figure 1C). The conjugation of Prot-S to the particles led to a 7 nm redshift of λ_{max}, in agreement with the presence of a protein corona around the AgNPs-X_4-Prot-S (Figure 1C). No additional significant modification of the LSPR band could be observed, indicating that the silver nanoparticles did not aggregate during the conjugation process. Hydrodynamic diameters of ∼35 and 67 nm were determined by DLS for AgNPs-X_4 and AgNPs-X_4-Prot-S, respectively (Figure 1D). These values are in good agreement with those reported in the literature for the increase of the hydrodynamic diameter of AgNPs due to the adsorption of biomolecules.[19] AgNPs-X_4 and AgNPs-X_4-Prot-S (before the addition of casein to be able to distinguish the signals from the Prot-S) were characterized by FT-IR spectroscopy (Figure 1E). The typical bands corresponding to the calixarene structure[31] (i.e., at ca. 1450 and 1050 cm^{-1} for the aromatic ring stretching and the symmetric COC_{Ar} stretching, respectively) were visible on both types of NPs, indicating that the calixarene layer remained stable during the conjugation step. Moreover, intense amide I and II bands (at 1650 and 1530 cm^{-1}, respectively) were visible after bioconjugation, confirming the presence of Prot-S at the AgNPs surface.

Finally, the stability of AgNPs-X_4-Prot-S in nondiluted plasma was evaluated by UV−vis spectroscopy. Strikingly, the thin calixarene-based coating conferred remarkable stability to the functionalized NPs as no change of the LSPR band was observed over a period of 1 h (Figure S1). This result highlights the fact that AgNPs-X_4-Prot-S are stable in complex media and opens the route to their use in real medical samples. It is worth noting that even in the absence of the protein corona, the particles (i.e., AgNPs-X_4) are stable in the presence of high salt concentration (1 M NaCl) (Figure S2).

3.2. General Principle of the Dipstick Assay for the Detection of Anti-SARS-CoV-2 IgG. Dipsticks composed of a nitrocellulose (NC) membrane and an absorbent pad were used for the development of the assay (Scheme 1). The test line (T) was coated with Anti-Human IgG and the control line (C) was coated with Anti-Rabbit IgG. AgNPs-X_4-Prot-S were used as the colorimetric reporter for the test line, whereas rabbit IgG-labeled AuNPs (AuNPs-citrate-Rabbit IgG; see the experimental part and Figure S3 for characterization) were used as the control colorimetric reporter. AgNPs-X_4-Prot-S were first incubated for 15 min with the plasma sample to form the SARS-CoV-2 antigen−antibody complexes. The dipstick was then immersed partially into the solution, and this latter migrated entirely toward the absorbent pad in 15 min. In the presence of Anti-SARS-CoV-2 IgG in the plasma sample, the AgNPs-X_4-ProtS-antibody complexes were captured by the IgG-binding proteins at the T line, generating a yellow-colored signal.

3.3. Evaluation of Silver Nanoparticles as a Colorimetric Reporter for Dipstick Assays. Before developing the AgNP-based dipstick assay for Anti-SARS-CoV-2 IgG, we first determined the minimal amount of silver nanoparticles required to obtain a signal unambiguously observable with the naked eye. For this, we designed a simplified dipstick assay based on AgNPs-X_4 modified with goat IgG (i.e., AgNPs-X_4-goat IgG) and a commercial dipstick only displaying a T line coated with protein A (no C line). The high affinity of protein

https://doi.org/10.1021/acs.analchem.2c00870
Anal. Chem. 2022, 94, 7383−7390

A for any IgG led to the immobilization of AgNPs-X_4-goat IgG and, as a result, to a yellow-colored T line that was observed at optical densities (OD) ranging from 0.4 to 0.01, which approximately corresponds to concentrations from 80 to 2 pM in AgNPs (Figure 2a,b).

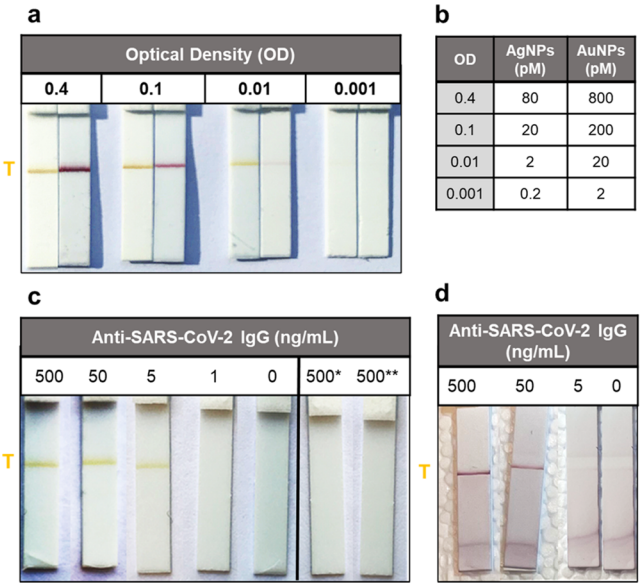

OD	AgNPs (pM)	AuNPs (pM)
0.4	80	800
0.1	20	200
0.01	2	20
0.001	0.2	2

Figure 2. (a) Picture of the protein A dipstick incubated with decreasing concentrations of either AgNPs-X_4-goat IgG or AuNPs-citrate-goat IgG. (b) Concentration values of AgNPs-X_4-goat IgG and AuNPs-citrate-goat IgG for the different investigated optical densities (OD) in PBS. Pictures of dipsticks used to detect different concentrations of Anti-SARS-CoV-2 IgG with either (c) AgNPs-X_4-Prot-S or (d) AuNPs-citrate-Prot-S. Labels represent the concentration in ng/mL. *: 500 ng/mL Anti-SARS-CoV-2 added to AgNPS-X_4. **: 500 ng/mL goat IgG to AgNPs-X_4-Prot-S.

For comparison purposes, similar experiments were performed with citrate-capped gold nanoparticles (AuNPs-citrate), as these NPs are the reference material used in commercial LFIAs. AuNPs-citrate of 20 nm were synthesized and modified with goat IgG (see the experimental part and Figure S4 for characterization). In this case, the goat IgG was adsorbed on AuNPs-citrate, as these particles are not stable enough to endure the EDC/NHS coupling conditions. It is worth noting that various AuNPs allowing covalent conjugation of antibodies have been reported in the literature, but commercial LFIAs are mostly based on AuNPs-citrate with adsorbed antibodies. The resulting AuNPs-citrate-goat IgG led, at optical densities of 0.4 and 0.1, to similar T line intensities to the corresponding AgNPs (Figure 2a,b). For an optical density of 0.01 or below, the signal of the silver nanoparticles was slightly more intense than the one of the AuNPs, probably because of the higher stability conferred by the calixarene coating. Despite a lower contrast of the yellow line obtained with AgNPs compared to the red one obtained with AuNPs on a white background, it is noteworthy that naked eye detection could be obtained with both sets of particles at similar OD. However, at the same OD, 10 times less AgNPs are used, as their molar extinction coefficient is ∼1 order of magnitude larger than that of their Au counterparts. Fewer reporter nanoparticles means that fewer biomolecules are needed to prepare them and, consequently, a reduced production cost for the LFIA. In other words, these first results confirmed that AuNPs could be advantageously replaced by calixarene-coated AgNPs for the design of dipstick assays or LFIAs.

The detection of monoclonal Anti-SARS-CoV-2 IgG with AgNPs-X_4-Prot-S was then evaluated in PBS, using a similar simplified dipstick system (i.e., with a half-strip displaying only a T line coated with Protein A). AgNPs-X_4-Prot-S with OD = 0.1 were mixed with buffered solutions of Anti-SARS-CoV-2 IgG at concentrations ranging from 0 to 500 ng/mL. After 15 min of incubation, the dipsticks were immersed in the solution and, 15 min later, the T line was analyzed (Figure 2c). According to this procedure, a limit of detection (LOD) of 5 ng/mL was determined, which corresponds to an Anti-SARS-CoV-2 IgG concentration of ca. 33 pM. Replicates can be found in the Supporting Information as well as the detection of intermediate values (i.e., 20, 10, and 2 ng/mL) that confirm a LOD of 5 ng/mL (Figure S5). Note that the visual observation results were confirmed through quantification of the signal intensity using ImageJ software[32] (Figure S5D).

Control experiments showed the high selectivity of the calixarene-coated AgNP system. Indeed, no colored T line was observed in the absence of Anti-SARS-CoV-2 IgG as well as upon the addition of (i) 500 ng/mL of Anti-SARS-CoV-2 IgG to unmodified AgNPs (i.e., AgNPs-X_4) or (ii) 500 ng/mL of goat IgG to AgNPs-X_4-Prot-S (Figure 2c). A comparison with the actual gold-standard material for LFIAs (i.e., AuNPs-citrate) with the protein-S adsorbed at its surface (i.e., AuNPs-citrate-Prot-S) was performed at similar ODs. A LOD of ca. 50 ng/mL was obtained with these particles (Figure 2d), as expected due to their inferior light extinction efficiency. Furthermore, a red trail was observed on all dipsticks, regardless of the concentration of Anti-SARS-CoV-2 IgG investigated, which could lead to false-positive errors. Taken together, these results show that (i) the calixarene-coated AgNPs are particularly well adapted to the design of efficient and highly sensitive LFIAs (with a sensitivity close to that of traditional ELISAs) and (ii) AgNPs-X4 are excellent colorimetric reporters for this type of system, as the LOD is reduced by 1 order of magnitude compared to classical AuNPs as a signal of at least similar intensity is obtained with 10 times fewer particles.

Finally, the detection of Anti-SARS-CoV-2 was performed with AgNPs-X_4-Prot-S stored at 4 °C for 6 months. The UV−vis spectra of both freshly prepared and aged AgNPs-X_4-Prot-S were almost identical (Figure 3). Very interestingly, 6-month-aged AgNPs-X_4-Prot-S remained capable of detecting 50 ng/mL of Anti-SARS-CoV-2 IgG in buffered solution with the same sensitivity and intensity as freshly prepared NPs (Figure 3, insets). This long shelf life of AgNPs-X_4-Prot-S can be explained by (i) the remarkably robust calixarene-based coating that strongly protects the AgNPs and (ii) the covalent immobilization of the Prot-S to the calixarene layer. This unique stability of calixarene-based AgNPs opens new perspectives in the field of RDTs, as particle shelf life is a common issue for LFIAs.

3.4. Optimization of the Detection of Anti-SARS-CoV-2 IgG in a Complex Matrix. The serological testing for COVID-19 in biological fluids (e.g., blood, plasma, or serum) is more complicated than in buffer solutions. Indeed, interferences between endogenous molecules and the AgNPs-Prot-S conjugates or with the proteins coating the dipstick could lead to a significant decrease in the signal intensity. As an example, the Protein A-coated strips could not be used for the detection of Anti-SARS-CoV-2 IgG in spiked

https://doi.org/10.1021/acs.analchem.2c00870
Anal. Chem. 2022, 94, 7383−7390

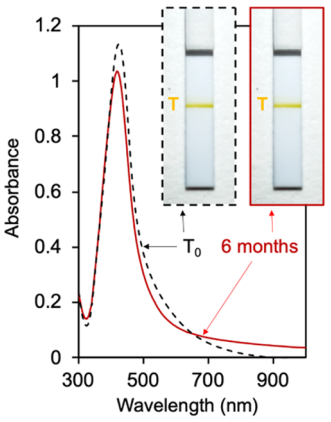

Figure 3. UV−vis spectra of an AgNPs-X_4-Prot-S dispersion, as freshly prepared (black dashed line) and 6 months later (red plain line). Insets show the pictures of the dipstick used for the detection of 50 ng/mL of Anti-SARS-CoV-2 in PBS with either AgNPs-X_4-Prot-S freshly prepared (black dashed box) or 6 months later (red box).

human plasma, as nearly no colored line could be observed even at a high concentration (5 μg/mL) of Anti-SARS-CoV-2 IgG (Figure S6). It was thus necessary to optimize the dipstick assay to allow detection in human plasma. Parameters such as the composition of the dipstick, type of membrane, and running buffer were screened. Best results were obtained when an intermediate-size pore CN140 membrane was used, and the test line was coated with goat Anti-human IgG (2 mg/mL) (Figure S7a,b). Moreover, it was shown that a blocking step of the membranes with a 0.5 wt % casein buffer was crucial to avoid false-positive results (Figure S7c). Finally, a running buffer containing 5 wt % BSA, 0.2 wt % Tween 20, 1 wt % PEG 6000, and 0.5× PBS was determined as the most suitable (see Table S1 for details on running buffer screening).

The optimized dipstick assay was then used for the detection of monoclonal Anti-SARS-CoV-2 IgG spiked in human plasma as depicted in Scheme 1. For this, 10 μL of plasma were mixed with 10 μL of AgNPs-X_4-Prot-S (OD = 5) dispersed in the running buffer. A yellow-colored T line was clearly observed until a concentration of Anti-SARS-CoV-2 IgG as low as 1.5 μg/mL (i.e., 10 nM) (Figure 4a). For lower concentrations,

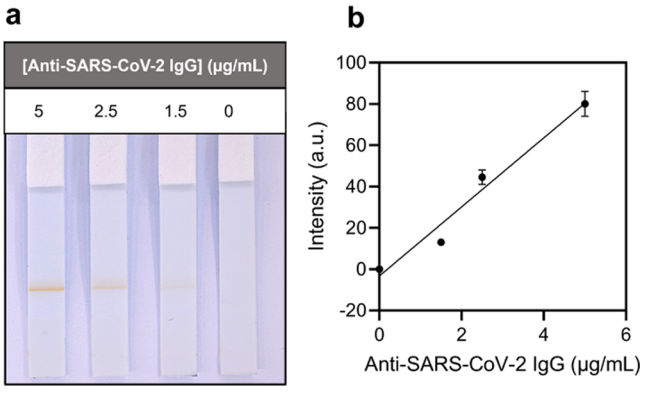

Figure 4. (a) Picture of the optimized dipstick assays used to detect different concentrations of monoclonal Anti-SARS-CoV-2 IgG spiked in human plasma. (b) Signal quantification from the pictures of the dipstick assays using ImageJ software (R^2 = 0.965). Note that the intensity values correspond to the average values of the three replicates.

the intensity of the yellow line was too low to be detected unambiguously with the naked eye. The lower LOD obtained in plasma (1.5 μg/mL) compared to the one that was obtained in buffer (5 ng/mL) may be explained by the numerous immunoglobulins that can interact with the anti-human IgG immobilized on the T line and interfere with the immobilization of the particles. The experiments were repeated three times with three independent batches of AgNPs-X_4-Prot-S, and the same LOD was determined by a panel of five observers (see Figure S8 for the pictures of the replicates). The signal intensity was also quantified using the ImageJ software,[32] confirming the LOD determined by visual observation (Figure 4b). It is worth mentioning that the median blood concentration of Anti-SARS-CoV-2 IgG is 16 μg/mL 20 days after the infection.[33] Similar experiments were performed with AuNPs-Prot-S, and false-positive results were obtained with plasma in the absence of Anti-SARS-CoV-2 IgG (Figure S9). This demonstrates the superiority of the AgNPs-X_4 as a colorimetric reporter for LFIAs. Also, it is worth noting that 6-month-aged AgNPs-X_4-Prot-S could still detect the Anti-SARS-CoV-2 IgG in human plasma with the same sensitivity and intensity (Figure S10).

3.5. Serological Testing for Anti-SARS-CoV-2 IgG in Real Human Samples. The detection conditions being optimized, the dipstick assay described in Scheme 1 was used for the serological testing of Anti-SARS-CoV-2 IgG in 15 positive clinical samples (P1−15, confirmed by RT-PCR), obtained from SARS-CoV-2-infected patients, as well as in 10 negative samples (N1−10). The positive samples were first analyzed by Wantai Ig Total ELISA to sort them into three distinct groups of five samples (i.e., high, moderate, and low total Ig concentration groups), depending on their concentration in Anti-SARS-CoV-2 immunoglobulins (IgG, IgM, IgA, etc.). Furthermore, ELISA quantification of Anti-SARS-CoV-2 IgG was performed for all samples to better rationalize the results obtained from the dipstick assays (see Table S2 for ELISA titer value of all samples). Anti-Rabbit IgG was immobilized on the control line to bind AuNPs modified with Rabbit IgG (Scheme 1). This Rabbit/Anti-Rabbit IgG system was chosen at the C line to (i) avoid any cross-reactivity and (ii) to easily distinguish the red-colored C line from the yellow-colored T line thanks to the different plasmonic properties of AuNPs and AgNPs. All samples were analyzed in duplicate, and the results were monitored independently by two operators.

The 10 negative samples N1−10 were first tested, and no yellow T line was observed, indicating a 100% specificity of the AgNPs-X_4-Prot-S (Figures 5b and S11). The 15 PCR positive samples were then tested with our dipstick assay, and 11 of them displayed a yellow band on the test line.

In the low-concentration Ig groups, four out of the five samples (P1−P4, Figure S12) displayed an IgG titer value below the cutoff level of ELISA (<12 AU/mL). For samples P1 and P3−P4, the IgG titer values were however higher than the values measured for PCR-negative samples. Interestingly, our lateral flow test presented a positive signal for these three samples, suggesting the detection of very small amounts of SARS-CoV-2 IgG, i.e., below the Elisa cutoff level. In the case of sample P2, the ELISA IgG titer value could not be distinguished from those obtained with PCR-negative samples (<3.8 AU/mL), which might explain why our dipstick assay was negative for that sample. Considering only the ELISA positive samples (titer above the threshold value), a yellow-

https://doi.org/10.1021/acs.analchem.2c00870
Anal. Chem. 2022, 94, 7383−7390

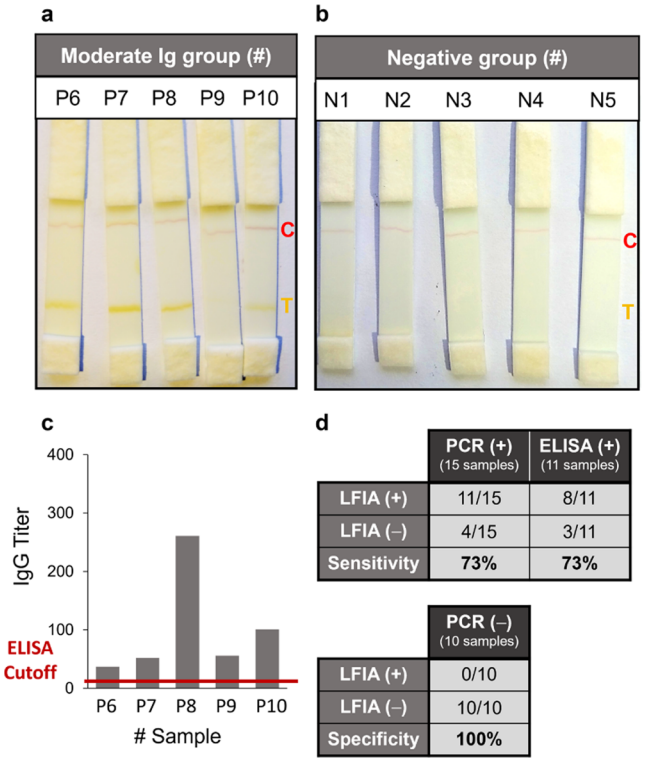

Figure 5. Pictures of dipstick assays for (a) the moderate Ig concentration positive sample group and (b) negative samples. (c) Quantification of Anti-SARS-CoV-2 IgG by Wantai ELISA for moderate concentration Ig group. (d) Analytical performance table.

colored test line was detected in 8 (P5−P8, P10, P12, P14−15) out of the 11 positive samples (P5−15), which corresponds to a sensitivity of 73% (see Figure 5a for the moderate concentration Ig group and Figure S12 for the two other groups). The corresponding ELISA titers of Anti-SARS-CoV-2 IgG for the moderate Ig group are displayed in Figure 5c. Note that no correlation between signal intensities and ELISA titers was observed. It is worth mentioning that a sensitivity of 73% is also obtained if all PCR positive samples (P1−15) are considered, including those showing the lowest IgG titers.

The comparison of the results of the dipstick assays as a function of PCR or ELISA analysis is summarized in Figure 5d. Regarding the ELISA positive samples, two of the three negative lateral flow tests belong to the high-concentration Ig group (P11 and P13) and one to the moderate group (P9). Therefore, the absence of a signal is not related to the limit of detection. A plausible explanation stems from the fact that other types of Ig (IgM, IgA) could bind to AgNPs-X_4-Prot-S or other types of IgG to the Anti-IgG line, respectively, interfering with and limiting the immobilization of the particles on the test line. Nevertheless, these results are extremely promising. Indeed, they represent one of the first examples of the use of a AgNP-based dipstick assay in the case of real clinical samples.[34] Moreover, our system exhibits analytical performances that are similar to those of systems based on AuNPs (61−69% sensitivity)[3−5] while using 10 times fewer particles to reach the same optical signal density (see Table S3 for some examples of commercial serological tests based on AuNPs and their sensitivity and specificity). Finally, we checked if our dipstick system could be used to design a real LFIA for the detection of Anti-SARS-CoV-2 IgG. To our delight, due to their high stability, the AgNPs-X_4-Prot-S could be dried on the conjugate pad, and the resulting LFIA led to a similar detection performance to the dipstick assays (see the Supporting Information for the design of the LFIAs and Figure S13).

4. CONCLUSIONS

We have shown that ultrastable silver nanoparticles coated by a thin layer of calix[4]arenes bearing carboxyl groups could be covalently conjugated with the SARS-CoV-2 Spike Protein (Prot-S) via the classical EDC/sulfo-NHS procedure. The resulting AgNPs-X_4-Prot-S are stable in complex matrixes such as human plasma and can be stored for months without any observable degradation, allowing their use for the development of LFIAs and the monitoring of real clinical samples. LODs of 5 ng/mL and 1.5 μg/mL were determined for the detection of Anti-SARS-CoV-2 IgG in buffer and in serum, respectively. These values are 10 times lower than those obtained with traditional AuNPs-citrate despite the fact that 10 times fewer AgNPs are used. These results suggest that the use of calixarene-coated AgNPs instead of AuNPs-citrate for the design of LFIAs could allow us to improve the limit of detection as well as the operating cost while ensuring a long shelf life (more than 6 months) to the particles. Our AgNP-based dipstick assay was used for the detection of SARS-CoV-2 IgG in clinical samples of patients who tested positive (RT-PCR) for SARS-CoV-2 infection. A high specificity was obtained as no false positive was detected. Moreover, a sensitivity of 73% was determined, which corresponds to that of the traditional AuNP-based LFIAs. All of these results highlight the superior optical properties of AgNPs, compared to AuNPs, and the ultrastability conferred by the calixarene coating to nanomaterials. These findings could benefit anyone developing LFIAs, regardless of the type of biomarker. Indeed, the high stability of the calixarene-based AgNPs and their conjugation capacity enable the covalent immobilization of a wide range of biomolecules such as proteins, antibodies, peptides, DNA aptamers, etc. Future work will be directed toward the extension of our strategy to other types of silver nanomaterials to develop LFIAs displaying colored lines with a better contrast on a white substrate.

■ ASSOCIATED CONTENT

Supporting Information

The Supporting Information is available free of charge at https://pubs.acs.org/doi/10.1021/acs.analchem.2c00870.

UV−vis and TEM characterization of AuNPs, detailed results about assay optimization, pictures of the dipstick assay for low- and high-Ig Tot groups, and ELISA titer tables of each clinical sample (PDF)

■ AUTHOR INFORMATION

Corresponding Authors

Gilles Bruylants − *Engineering of Molecular NanoSystems, Ecole Polytechnique de Bruxelles, Université libre de Bruxelles (ULB), B-1050 Brussels, Belgium;* orcid.org/0000-0003-1752-5826; Email: Gilles.Bruylants@ulb.be

Ivan Jabin − *Laboratoire de Chimie Organique, Université libre de Bruxelles (ULB), B-1050 Brussels, Belgium;* orcid.org/0000-0003-2493-2497; Email: Ivan.Jabin@ulb.be

https://doi.org/10.1021/acs.analchem.2c00870
Anal. Chem. 2022, 94, 7383−7390

Authors

Bryan Gosselin − *Engineering of Molecular NanoSystems, Ecole Polytechnique de Bruxelles, Université libre de Bruxelles (ULB), B-1050 Brussels, Belgium; Laboratoire de Chimie Organique, Université libre de Bruxelles (ULB), B-1050 Brussels, Belgium*

Maurice Retout − *Engineering of Molecular NanoSystems, Ecole Polytechnique de Bruxelles, Université libre de Bruxelles (ULB), B-1050 Brussels, Belgium*

Raphaël Dutour − *Engineering of Molecular NanoSystems, Ecole Polytechnique de Bruxelles, Université libre de Bruxelles (ULB), B-1050 Brussels, Belgium*

Ludovic Troian-Gautier − *Laboratoire de Chimie Organique, Université libre de Bruxelles (ULB), B-1050 Brussels, Belgium;* orcid.org/0000-0002-7690-1361

Robin Bevernaegie − *Laboratoire de Chimie Organique, Université libre de Bruxelles (ULB), B-1050 Brussels, Belgium*

Sophie Herens − *Service de Biologie Clinique, Clinique CHC MontLégia, 4000 Liège, Belgium*

Philippe Lefèvre − *Service de Biologie Clinique, Hôpital de Marche, Groupe VIVALIA, 6900 Marche en Famenne, Belgium*

Olivier Denis − *Service Immune Response, Sciensano, 1180 Brussels, Belgium*

Complete contact information is available at: https://pubs.acs.org/10.1021/acs.analchem.2c00870

Author Contributions

#B.G. and M.R. contributed equally.

Notes

The authors declare the following competing financial interest(s): L.T.-G. and M.R. were postdoctoral researchers for X4C, respectively, from October 2014 to September 2015 and from August 2020 to January 2021. I.J. is a shareholder of X4C. I.J. and G.B. are consultants for X4C.

■ ACKNOWLEDGMENTS

This research was supported by the Fonds pour la formation à la Recherche dans l'Industrie et dans l'Agriculture (FRIA-FRS) (PhD grant to B.G.), the Fonds de la Recherche Scientifique (FRS-FNRS) (postdoctoral grant to L.T.-G.), the "Actions de Recherches Concertées" of the Fédération Wallonie-Bruxelles and the ULB (PhD grant to M.R. and R.D.), the "Appel à projets Spécial COVID-19 − ULB", the Green Chemistry Program of Innoviris (postdoctoral grant to R.B.) and the "Fondation Jaumotte-Demoulin". The authors thank Dr. Vincent Lejeune (Hôpital de Marche, Groupe VIVALIA) for his help in getting the clinical samples.

■ REFERENCES

(1) Liu, G.; Rusling, J. F. *ACS Sens.* **2021**, *6*, 593−612.
(2) Song, Q.; Sun, X.; Dai, Z.; Gao, Y.; Gong, X.; Zhou, B.; Wu, J.; Wen, W. *Lab Chip* **2021**, *21*, 1634−1660.
(3) Wen, T.; Huang, C.; Shi, F.-J.; Zeng, X.-Y.; Lu, T.; Ding, S.-N.; Jiao, Y.-J. *Analyst* **2020**, *145*, 5345−5352.
(4) Huang, C.; Wen, T.; Shi, F.-J.; Zeng, X.-Y.; Jiao, Y.-J. *ACS Omega* **2020**, *5*, 12550−12556.
(5) Zeng, L.; Li, Y.; Liu, J.; Guo, L.; Wang, Z.; Xu, X.; Song, S.; Hao, C.; Liu, L.; Xin, M.; Xu, C. *Mater. Chem. Front.* **2020**, *4*, 2000−2005.
(6) Di Nardo, F.; Chiarello, M.; Cavalera, S.; Baggiani, C.; Anfossi, L. *Sensors* **2021**, *21*, No. 5185.
(7) Soh, J. H.; Chan, H.-M.; Ying, J. Y. *Nano Today* **2020**, *30*, No. 100831.
(8) Paramelle, D.; Sadovoy, A.; Gorelik, S.; Free, P.; Hobley, J.; Fernig, D. G. *Analyst* **2014**, *139*, 4855.
(9) Liu, X.; Atwater, M.; Wang, J.; Huo, Q. *Colloids Surf., B* **2007**, *58*, 3−7.
(10) Daruich De Souza, C.; Ribeiro Nogueira, B.; Rostelato, M. E. C. M. *J. Alloys Compd.* **2019**, *798*, 714−740.
(11) Jazayeri, M. H.; Amani, H.; Pourfatollah, A. A.; Pazoki-Toroudi, H.; Sedighimoghaddam, B. *Sens. Bio-Sens. Res.* **2016**, *9*, 17−22.
(12) Retout, M.; Brunetti, E.; Valkenier, H.; Bruylants, G. *J. Colloid Interface Sci.* **2019**, *557*, 807−815.
(13) Biju, V. *Chem. Soc. Rev.* **2014**, *43*, 744−764.
(14) Liu, Y.; Zhan, L.; Qin, Z.; Sackrison, J.; Bischof, J. C. *ACS Nano* **2021**, *15*, 3593−3611.
(15) Xu, Y.; Liu, Y.; Wu, Y.; Xia, X.; Liao, Y.; Li, Q. *Anal. Chem.* **2014**, *86*, 5611−5614.
(16) Tran, V.; Walkenfort, B.; König, M.; Salehi, M.; Schlücker, S. *Angew. Chem., Int. Ed.* **2019**, *58*, 442−446.
(17) Bhardwaj, J.; Sharma, A.; Jang, J. *Biosens. Bioelectron.* **2019**, *126*, 36−43.
(18) Lee, J.-S.; Lytton-Jean, A. K. R.; Hurst, S. J.; Mirkin, C. A. *Nano Lett.* **2007**, *7*, 2112−2115.
(19) Yen, C.-W.; de Puig, H.; Tam, J. O.; Gómez-Márquez, J.; Bosch, I.; Hamad-Schifferli, K.; Gehrke, L. *Lab Chip* **2015**, *15*, 1638−1641.
(20) Anfossi, L.; Di Nardo, F.; Russo, A.; Cavalera, S.; Giovannoli, C.; Spano, G.; Baumgartner, S.; Lauter, K.; Baggiani, C. *Anal. Bioanal. Chem.* **2019**, *411*, 1905−1913.
(21) Pinzaru, I.; Coricovac, D.; Dehelean, C.; Moacă, E.-A.; Mioc, M.; Baderca, F.; Sizemore, I.; Brittle, S.; Marti, D.; Calina, C. D.; Tsatsakis, A. M.; Şoica, C. *Food Chem. Toxicol.* **2018**, *111*, 546−556.
(22) Wang, Y.; van Asdonk, K.; Zijlstra, P. *Langmuir* **2019**, *35*, 13356−13363.
(23) Retout, M.; Jabin, I.; Bruylants, G. *ACS Omega* **2021**, *6*, 19675−19684.
(24) Mattiuzzi, A.; Jabin, I.; Mangeney, C.; Roux, C.; Reinaud, O.; Santos, L.; Bergamini, J.-F.; Hapiot, P.; Lagrost, C. *Nat. Commun.* **2012**, *3*, No. 1130.
(25) Troian-Gautier, L.; Mattiuzzi, A.; Reinaud, O.; Lagrost, C.; Jabin, I. *Org. Biomol. Chem.* **2020**, *18*, 3624−3637.
(26) Li, D.; Luo, Y.; Onidas, D.; He, L.; Jin, M.; Gazeau, F.; Pinson, J.; Mangeney, C. *Adv. Colloid Interface Sci.* **2021**, *294*, No. 102479.
(27) Retout, M.; Gosselin, B.; Mattiuzzi, A.; Ternad, I.; Jabin, I.; Bruylants, G. *ChemPlusChem* **2021**, *87*, No. e202100450.
(28) Lee, H.-K.; Lee, B.-H.; Seok, S.-H.; Baek, M.-W.; Lee, H.-Y.; Kim, D.-J.; Na, Y.-R.; Noh, K.-J.; Park, S.-H.; Kumar, D. N.; Kariwa, H.; Nakauchi, M.; Heo, S.-J.; Park, J.-H. *J. Vet. Sci.* **2010**, *11*, No. 165.
(29) Troian-Gautier, L.; Valkenier, H.; Mattiuzzi, A.; Jabin, I.; den Brande, N. V.; Mele, B. V.; Hubert, J.; Reniers, F.; Bruylants, G.; Lagrost, C.; Leroux, Y. *Chem. Commun.* **2016**, *52*, 10493−10496.
(30) Doyen, M.; Bartik, K.; Bruylants, G. *J. Colloid Interface Sci.* **2013**, *399*, 1−5.
(31) Blond, P.; Bevernaegie, R.; Troian-Gautier, L.; Lagrost, C.; Hubert, J.; Reniers, F.; Raussens, V.; Jabin, I. *Langmuir* **2020**, *36*, 12068−12076.
(32) Parolo, C.; Sena-Torralba, A.; Bergua, J. F.; Calucho, E.; Fuentes-Chust, C.; Hu, L.; Rivas, L.; Álvarez-Diduk, R.; Nguyen, E. P.; Cinti, S.; Quesada-González, D.; Merkoçi, A. *Nat. Protoc.* **2020**, *15*, 3788−3816.
(33) Ma, H.; Zeng, W.; He, H.; Zhao, D.; Jiang, D.; Zhou, P.; Cheng, L.; Li, Y.; Ma, X.; Jin, T. *Cell. Mol. Immunol.* **2020**, *17*, 773−775.
(34) Liu, H.; Dai, E.; Xiao, R.; Zhou, Z.; Zhang, M.; Bai, Z.; Shao, Y.; Qi, K.; Tu, J.; Wang, C.; Wang, S. *Sens. Actuators, B* **2021**, *329*, No. 129196.